Prehydrodynamic evolution and its signatures in final-state heavy-ion observables

T. Nunes da Silva,[1,*] D. Chinellato,[2,†] G. S. Denicol,[3,‡] M. Hippert,[2,4,§] M. Luzum,[5,‖] J. Noronha,[4,¶] W. Serenone,[2,#] and J. Takahashi[2,**]
(ExTrEMe Collaboration)
[1]*Departamento de Física, Centro de Ciências Físicas e Matemáticas, Universidade Federal de Santa Catarina, Campus Universitário Reitor João David Ferreira Lima, Florianópolis 88040-900, Brazil*
[2]*Instituto de Física Gleb Wataghin, Universidade Estadual de Campinas, R. Sérgio Buarque de Holanda, 777, Campinas 13083-859, Brazil*
[3]*Instituto de Física, Universidade Federal Fluminense, Av. Milton Tavares de Souza, Niterói 24210-346, Brazil*
[4]*Illinois Center for Advanced Studies of the Universe & Department of Physics, University of Illinois at Urbana-Champaign, Urbana, Illinois 61801, USA*
[5]*Instituto de Física, Universidade de São Paulo, R. do Matão, 1371, São Paulo 05508-090, Brazil*

(Received 11 June 2020; accepted 12 April 2021; published 18 May 2021)

We investigate the effects of prehydrodynamic evolution on final-state observables in heavy-ion collisions using state-of-the art event simulations coupled to different prehydrodynamic scenarios, which include the recently developed effective kinetic transport theory evolution model KøMPøST. Differential flow observables are found to be mostly insensitive to the details of prehydrodynamic evolution. The main effect we observe is in the p_T spectra, particularly the mean transverse momentum. However, at least part of this effect is a consequence of the underlying conformal invariance assumption currently present in such approaches, which is known to be violated in the temperature regime probed in heavy-ion collisions. This assumption of early time conformal invariance leads to an artificially large out-of-equilibrium bulk pressure when switching from (conformal) prehydrodynamic evolution to hydrodynamics (using the nonconformal QCD equation of state), which in turn increases the transverse momentum. Our study indicates that a consistent treatment of prehydrodynamic evolution in heavy-ion collisions requires the use of nonconformal models of early time dynamics.

DOI: 10.1103/PhysRevC.103.054906

I. INTRODUCTION

Under extreme conditions of density and temperature, quantum chromodynamics (QCD) [1,2] predicts the existence of the quark-gluon plasma (QGP) [3], a state of matter where quarks and gluons are not confined into hadrons. Naturally occurring examples where the QGP is formed [4] include the primordial universe and, possibly, the interior of ultra compact astrophysical objects such as neutron stars [5]. The experimental program of relativistic heavy-ion collisions has been developed with the goal of producing and characterizing this extreme state of matter, shedding an important light on fundamental aspects of the strong interaction [6–11]. These experiments have provided mounting evidence that, at least in collisions between large nuclei, short-lived QGP matter is formed and exhibits collective behavior [6–13].

Given the limitation of lattice QCD methods to problems in equilibrium [14], the large scale dynamical evolution of the QGP formed in heavy-ion collisions has been described using relativistic viscous hydrodynamics [15,16] (for a review, see Ref. [17]). However, because the QGP cools down as it expands at relativistic speeds, it will eventually hadronize. In practice, only the final stable hadrons resulting from the decays of the zoo of exotic states formed during hadronization is detected by the experiments, i.e., the properties of the QGP must be extracted without its direct detection. Phenomenology has dealt with this by employing *hybrid models* (see, for instance, Ref. [18]), in which different stages of the collision event are successively modelled using different numerical models. These stages are:

(i) *initial hard scattering* between nuclei, which produces hot and dense QCD matter;
(ii) *hydrodynamization* during which matter approaches a fluid behavior;
(iii) *hydrodynamical evolution*, during which the QGP evolves according to relativistic viscous hydrodynamics, including hadronization as the QGP cools down and hadrons are formed;
(iv) *interacting hadron gas evolution* as the final stage for the resulting system of hadronic resonances, during which unstable states decay.

*t.j.nunes@ufsc.br
†daviddc@g.unicamp.br
‡gsdenicol@id.uff.br
§hippert@ifi.unicamp.br
‖mluzum@usp.br
¶jn0508@illinois.edu
#serenone@ifi.unicamp.br
**jun@ifi.unicamp.br

When building a simulation chain for a hybrid model, the above steps are typically mapped into:

(i) *initial condition generation code*, which models the initial state entropy (energy) density profile resulting from the collisions between the nuclei [19–30];
(ii) *pre-equilibrium dynamics model*, which models the early time dynamics of the system, during which it evolves from an out-of-equilibrium state to another state where relativistic viscous hydrodynamics is assumed to hold [27,28,31–34];
(iii) *viscous relativistic hydrodynamics code*, which is typically the workhorse of such models, describing the dynamical evolution of the QGP and its transition into a hadronic system [15,16,35–40];
(iv) *particlization code*, which translates the hydrodynamical degrees of freedom at freezeout into hadrons, by sampling the hydrodynamic freezeout hypersurface [41–44];
(v) *hadron cascade model*, which propagates the interacting gas of hadrons and handles resonance decays [19,20,45–47];

While these setups generally reproduce experimental data with considerable precision, there remain shortcomings in the understanding of several theoretical aspects underlying such chains of numerical codes. One of these pressing questions is to understand how the dense and hot matter formed immediately after the collision approaches fluid behavior, a process usually referred to as *hydrodynamization* (for a review, see Refs. [48,49]). This stage of relativistic heavy-ion collisions is under active scrutiny also by experimentalists, by means of studies of collisions of the so-called *small systems*, such as proton-nucleous (p-A) and proton-proton (p-p), in which hints of collective behavior have been found [50,51].

In this work, a state-of-the art hybrid model with different pre-equilibrium dynamical scenarios is used to investigate how the latter affect final-state observables. In particular, we show that while differential flow observables, including a principal component analysis of the two-particle correlation matrix in transverse momentum, are practically insensitive to the details of pre-equilibrum dynamics, there is a nonnegligible effect on the transverse momentum spectra, which is also reflected in the integrated flow. We show evidence that at least part of this effect (and possibly most) originates from the simplifying assumption of conformal invariance in the pre-equilibrium dynamics models used in the simulation chain, which results in a large out-of-equilibrium bulk pressure at the matching with the hydrodynamical model. The resulting signature of this extra bulk pressure in final-state observables is precisely the increase of mean transverse momentum.

In Sec. II we briefly review the pre-equilibrium models that are employed in this work. Section III gives the details of our numerical setup. Our results can be found in Sec. IV, followed by our conclusions and outlook. *Definitions:* We use natural units, $\hbar = c = k_B = 1$, and a mostly plus signature for the Minkowski metric.

II. PRE-EQUILIBRIUM MODELING

As explained above, there is a strong interconnection between the different stages of a heavy-ion collision. Therefore, improving our understanding of each of the above stages has a considerable impact in our comprehension of the global picture. In this sense, a remaining key piece of the puzzle is to understand what mechanism, if any, brings the highly out-of-equilibrium matter formed immediately after the collision to a state where a hydrodynamical description may be valid.

Hydrodynamical studies (and hybrid models) have directly employed, as initial conditions for hydrodynamics, results from models based on the color-glass condensate framework [52] such as IP-Glasma [27,28], string/transport approaches such as UrQMD [19,20], AMPT [23,24], EPOS [25], NeXus [26], and SMASH [30] and also parametrical models of entropy (energy) deposition such as the Glauber model [21,22] and T$_\mathrm{R}$ENTo [29].

More recently, effective models have been employed to bridge the gap between such models and the initial (full) energy-momentum tensor at the start of hydrodynamics. In practice, such models aim at describing the system from a very early initial time τ_0, up to the time at which a hydrodynamical evolution is valid τ_{hydro}, by evolving the resulting profiles from the preceding deposition models for $\tau_0 < \tau < \tau_{\mathrm{hydro}}$.

As a simple example, consider a boost invariant [53] system of on-shell noninteracting massless partons that emerge isotropically from an initial hard scattering at time τ_0 [31,32]. The energy-momentum tensor of such a system at a spacetime point $(\tau, \mathbf{x})$ can then be obtained by integrating the initial energy density of partons (multiplied by τ) in the transverse plane, $n(\tau_0, x, y)$ over a ring of radius $c\Delta\tau = c(\tau - \tau_0)$,

$$T^{\mu\nu}(x, y) = \frac{1}{\tau} \int d\phi \, \hat{p}^{\mu} \hat{p}^{\nu} n(x - \Delta\tau \cos\phi, y - \Delta\tau \sin\phi), \tag{1}$$

where $\hat{p}^{\mu} \equiv p^{\mu}/p_T$ is a transverse-momentum unit vector, ϕ is the transverse azimuthal angle, and $\tau = \sqrt{t^2 - z^2}$. This procedure effectively smooths out the energy density of the system and, in a simple model of thermalization, this free streaming dynamics is interrupted at a time $\tau_{\mathrm{fs}} > \tau_0$ at which the system is assumed to suddenly attain local thermal equilibrium. Clearly, this sudden transition from a model with zero coupling to a model with finite (strong) coupling is unphysical and, thus, it may only be used as a zeroth order approximation of the pre-equilibrium dynamics.

Recently, a step forward towards a more realistic scenario was proposed in Refs. [33,34] where the description of the evolution of the out-of-equilibrium energy-momentum tensor during this period is done via an effective kinetic theory (EKT) of weakly coupled QCD [54], using a leading-order pure-gluon QCD collision kernel. In this new framework, following general ideas from the color-glass condensate, the dynamics of the system at early times after the collision is assumed to be determined by Yang-Mills equations for the classical gluon fields. Once the gluonic fields become sufficiently dilute, at a time τ_{EKT}, the subsequent evolution of the system becomes dominated by effective kinetic processes

which ultimately drive the resulting plasma towards a state where hydrodynamics may be applicable.

The model mentioned above, called KøMPøST, aims at bridging this gap between the early time dynamics and the conditions necessary for the start of hydrodynamical simulations. In practice, between a time $\tau_{\rm EKT}$, at which kinetic processes become dominant in the evolution of the plasma, and the subsequent $\tau_{\rm hydro}$, at which the plasma becomes describable by relativistic hydrodynamics, the energy-momentum tensor of the system is evolved according to a linear response formalism: the energy-momentum tensor in the causal past of a given point within the out-of-equilibrium initial condition is written as a sum between a background local average plus small perturbations [33,34]. The public version of KøMPøST allows for evolving a given initial condition using either the full EKT evolution or its free streaming limit. In fact, in this study, we will show results from both evolution models and investigate their differences.

In both pre-equilibrium models, namely KøMPøST and free-streaming, the system is conformal invariant. Therefore, $T^{\mu\nu}$ can be decomposed (using the so-called Landau frame [55]) in terms of the usual hydrodynamic variables, i.e., the energy density e, flow velocity u^μ, and shear-stress tensor $\pi^{\mu\nu}$ in the following way,

$$T^{\mu\nu} = e\left(u^\mu u^\nu + \frac{\Delta^{\mu\nu}}{3}\right) + \pi^{\mu\nu}, \tag{2}$$

where $\Delta^{\mu\nu} \equiv g^{\mu\nu} + u^\mu u^\nu$. This energy-momentum tensor is then used to obtain the initial conditions for the corresponding fields in the hydrodynamical simulation. We note that the underlying conformal invariance implies that $T^{\mu\nu}$ is traceless and, in the aforementioned models, the bulk viscous pressure, Π, must vanish and the equation of state is simply given by $e = 3p$. In fluid-dynamical simulations, the equation state is not conformal and there is no reason to assume that $T^{\mu\nu}$ is traceless. However, to guarantee energy-momentum conservation in the transition from the pre-equilibrium models to the fluid-dynamical description, one introduces a nonzero bulk viscous pressure to compensate that $e - 3p \neq 0$ in QCD. In this case, one must have $e - 3p - 3\Pi = 0$ and this conditions sets the initial value of Π for the subsequent fluid-dynamical simulation. This discontinuity in the thermodynamic pressure and bulk viscous pressure is a nonwanted feature in all pre-equilibrium models that assume conformal invariance. The consequences of such spurious approximation shall be discussed later in this paper.

III. NUMERICAL SETUP

We have simulated collisions of Pb-Pb nuclei with center of mass energy $\sqrt{s_{NN}} = 2.76$ TeV across all centralities using a hybrid model composed of:

(i) T_RENTo, a parametric model for generating an initial entropy profile after the nucleus-nucleus collision [29];
(ii) KøMPøST, the kinetic theory model described in the previous section that simulates pre-equilibrium dynamics [33,34];
(iii) MUSIC, an event-by-event relativistic second-order viscous hydrodynamics [56,57] code [38–40,58];
(iv) iSS, a hadronization hypersurface sampler [37];
(v) UrQMD, a hadronic cascade model [19,20].

The parameters employed in the generation of the initial entropy profile in T_RENTo were obtained from recent Bayesian analyses in Refs. [59,60], *except* for the overall normalization factor, which was obtained by matching the resulting multiplicity of charged particles to experimental data from the ALICE Collaboration [61].

This initial entropy density is then converted to energy density using a lattice QCD-based equation of state (details of the equation of state will be provided below) and used as an initial condition at time $\tau_0 = 0.2$ fm. The full energy momentum tensor is then chosen to be diagonal, and is used either as an initial condition for viscous hydrodynamics at τ_0 or evolved using KøMPøST up to a later time $\tau_{\rm hydro} = 1.2$ fm and inserted into hydrodynamics.

In our study, MUSIC was used to perform $2D + 1$ (boost invariant) viscous hydrodynamical simulations of the hydrodynamical stage, including shear and bulk viscosities. We followed [60] and parametrized the shear viscosity to entropy density ratio as

$$(\eta/s)(T) = (\eta/s)_{\rm min} + (\eta/s)_{\rm slope}(T - T_c)(T/T_c)^{(\eta/s)_{\rm crv}}, \tag{3}$$

while the bulk viscosity to entropy density ration is given by

$$(\zeta/s)(T) = \frac{(\zeta/s)_{\rm max}}{1 + \left(\frac{T-(\zeta/s)_{T_0}}{(\zeta/s)_{\rm width}}\right)^2}. \tag{4}$$

For the shear viscosity, $(\eta/s)_{\rm min}$ is the minimum value at T_c, $(\eta/s)_{\rm slope}$ is a slope above T_c, and $(\eta/s)_{\rm crv}$ is a curvature parameter. The expression for the bulk viscosity is a Cauchy distribution, which parametrizes a symmetric peak with three free parameters: a maximum value, $(\zeta/s)_{\rm max}$, its width, $(\zeta/s)_{\rm width}$, and center, $(\zeta/s)_{T_0}$. The set of parameters utilized in this model was inspired by the optimal parameters recently obtained by Bayesian analysis [59,60], given the similarities between the models employed in both works. However, due to some differences between the models, namely in the choice of equation of state and in the realization of the free streaming stage, these parameters have to be re-adjusted to describe the charged hadron mean transverse-momentum and the flow observables. We improved the description of such observables in our model by modifying the minimum value of shear viscosity to $(\eta/s)_{\rm min} = 0.04$, and the maximum value of bulk viscosity to $(\zeta/s)_{\rm max} = 0.14$. The remaining transport coefficients in MUSIC are taken from Refs. [40,58].

The equilibrium equation of state we used is the parametrization constructed by Huovinen and Petreczky known as s95p-v1.2 [62]. For temperatures below 184 MeV, this equation of state is based on a hadron resonance gas. Above this temperature, it employs lattice results by Bazavov *et al.* [63]. This version of the equation of state contains the same particle species as UrQMD. We leave the implementation of a more realistic version of the QCD equation of state, e.g., the one used in Refs. [64,65], to future work.

The transition from the hydrodynamical degrees of freedom to the hadron gas is made via the Cooper-Frye formalism [41], including viscous corrections, in a constant temperature hypersurface. Such particlization temperature is taken from the aforementioned Bayesian analysis [60] and is $T_{\rm FO} = 151$ MeV. The viscous corrections employed in the Cooper-Frye procedure are taken from [40,58]. The freeze-out hypersurfaces from hydrodynamics have been repeatedly sampled until 5×10^5 particles were acquired per unity rapidity. The final configurations of stable particles were then stored in a ROOT-based C++ class, and finally used for data analysis and the calculation of observables.

To disentangle the effects of pre-equilibrium dynamics over the observables of interest, three main scenarios have been studied. In all three cases, results from the T$_{\rm R}$ENTo model are regarded as an initial entropy density profiles at time $\tau = 0.2$. The scenarios differ in the following manner:

(i) In Scenario A, the initial entropy density profile generated by T$_{\rm R}$ENTo is converted to energy density, using the QCD equation of state, and utilized directly as the initial condition for hydrodynamical evolution, starting at time $\tau_0 = 0.2$ fm. The transverse velocity, initial shear-stress tensor, and bulk pressure are chosen to vanish;

(ii) In Scenario B, the same initial energy profile from Scenario A is used. The energy-momentum tensor is determined according to $T^{\mu\nu} = \mathrm{diag}(e, e/2, e/2, 0)$, with e constructed using T$_{\rm R}$ENTo, as described above, and then evolved using the free streaming limit of KøMPøST from $\tau_0 = 0.2$ fm until $\tau_{\rm hydro} = 1.2$ fm, at which point the hydrodynamical evolution is started;

(iii) Scenario C, is analogous to Scenario B, but now the the initial profile is propagated from $\tau_0 = 0.2$ fm until $\tau_{\rm hydro} = 1.2$ fm using the KøMPøST effective kinetic theory model [33,34] with $\eta/s = 0.16$, after which hydrodynamic evolution is initiated.

We have employed the same initial T$_{\rm R}$ENTo profiles for the three scenarios above. The only difference is a rescaling of the overall normalization factor in the model. In current models for initial conditions the overall normalization factor is an unknown free parameter that is chosen so that the correct final multiplicity is obtained. We follow this procedure and adjust the energy normalization so that all the scenarios yield a charged particle multiplicity at central events consistent with experimental data. Specifically, the initial energy from Scenario A is multiplied by a factor 0.82 for Scenario B and 0.975 for Scenario C. That is, the free streaming evolution tends to increase the final particle multiplicity compared to hydrodynamic evolution, while the EKT evolution tends to decrease it.

For each of these cases, the resulting multiplicities of final charged particles are shown as a function of centrality, in Fig. 1, where they are compared to experimental results from the ALICE collaboration [61]. These results were also used as a consistency check for the model.

The parameters utilized in the simulations are summarized in the table below.

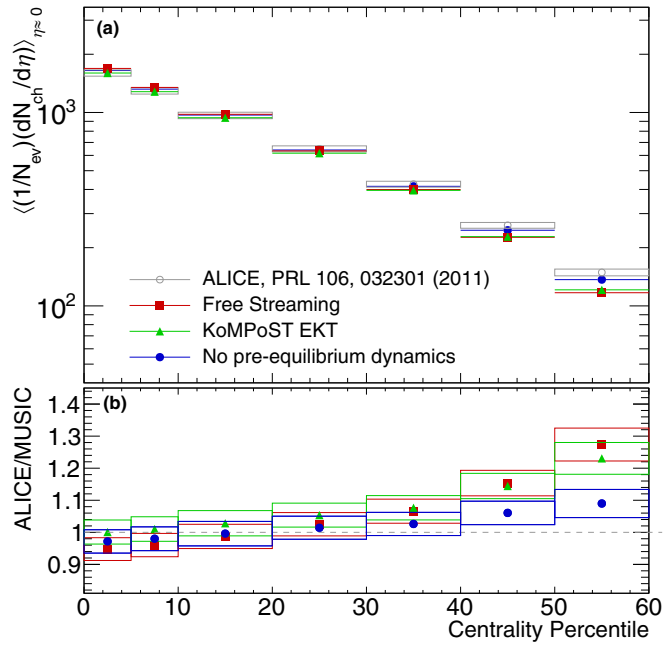

FIG. 1. (a) Final multiplicity of charged particles as a function of centrality for all of the prehydrodynamical scenarios under consideration. (b) We also show the ratio between the experimental results [61] and results from our simulations.

Initial Condition		QGP Properties	
Normalization (Scenario A)	269.05	$(\eta/s)_{\rm min}$	0.04
Normalization (Scenario B)	234.70	$(\eta/s)_{\rm slope}$	1.11 (1/GeV)
Normalization (Scenario C)	279.08	$(\eta/s)_{\rm cvr}$	−0.48
p	0.007	$(\zeta/s)_{\rm max}$	0.14
$\sigma_{\rm fluct}$	0.918	$(\zeta/s)_{\rm width}$	0.022 GeV
w	0.956 fm	$(\zeta/s)_{T_0}$	183 MeV
$d_{\rm min}$	1.27 fm	$T_{\rm switch}$	151 MeV

IV. RESULTS

We start by presenting results for the differential p_T spectra of charged particles for the three scenarios under consideration, across several centrality ranges. The results are presented in Fig. 2, in which it is already possible to notice the effect of the inclusion of pre-equilibrium dynamics on the final momentum spectrum, across all centralities. To make the visualization of this effect clearer, we also show in Fig. 3 ratios between scenarios B and C and the standard scenario A. It is then clear that the addition of KøMPøST, either in EKT or free streaming mode, causes a significant change in the shape of the transverse momentum spectra, resulting in a smaller spectrum at low p_T that progressively becomes larger at higher values of p_T. The relative magnitude of the effect is larger in more peripheral events. Overall, the net result of the effect is an increase in average transverse momentum, which is shown, per centrality class, in Fig. 4 for three particle species (and their corresponding antiparticles): pions, kaons,

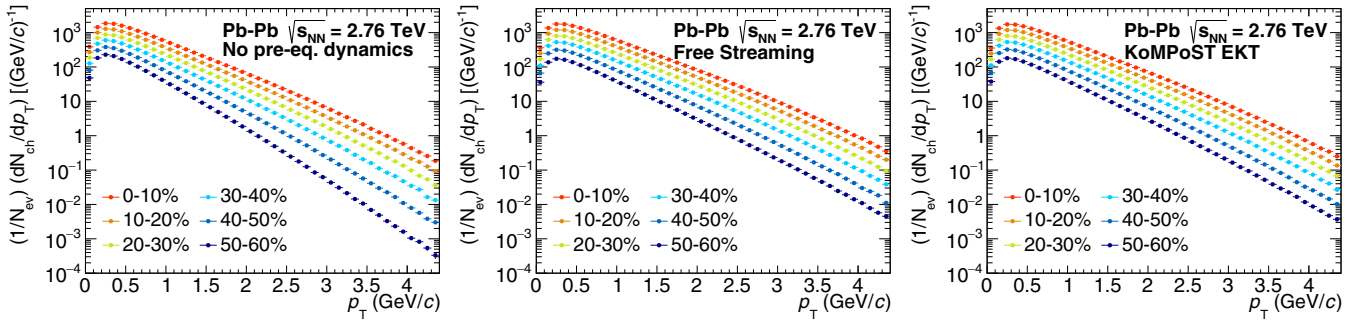

FIG. 2. Spectra of momentum of charged particles in the transverse plane for the three scenarios under consideration: A (left), B (middle), and C (right).

and protons. Therefore, both the free streaming limit and the EKT scenario behave similarly, with larger mean transverse momenta compared to the hydrodynamic scenario. We now analyze the usual anisotropic flow observables v_n, which are the coefficients of the Fourier expansion of the probability distribution of finding a particle at rapidity y with transverse momentum p_T in the azimutal angle ϕ:

$$E\frac{dN}{d^3p} \equiv \frac{1}{2\pi}\frac{\sqrt{m^2+p_T^2\cosh(\eta)^2}}{p_T\cosh(\eta)}\frac{dN}{p_T dp_T d\eta} \times\left[1+\sum_{n=1}^{\infty} v_n(p_T,\eta)\cos n(\phi-\Psi_n)\right]. \quad (5)$$

We have extracted the anisotropic flow coefficients from the simulated events following the Q-cumulants formalism, which uses multiparticle azimuthal correlation to avoid dealing with measurements of event plane angles. Explicitly, the flow coefficients can be related to the two-particle correlation function for a given centrality through the relation [66,67]

$$v_n\{2\} = \sqrt{\langle v_n\rangle^2} = \sqrt{\langle\langle e^{in(\phi_1-\phi_2)}\rangle\rangle}. \quad (6)$$

We have followed the usual computational strategy and built the so-called Q vector [67],

$$Q_n = \sum_{i=1}^{M} e^{in\phi_i}, \quad (7)$$

so that the v_n coefficients extracted from two particle correlations is given by

$$v_n\{2\} = \sqrt{\left\langle\frac{|Q_n|^2-M}{M(M-1)}\right\rangle}. \quad (8)$$

Results for the integrated $v_n\{2\}$ in the transverse momentum interval $0.2 < p_t < 3.0$ GeV for the three scenarios are shown in Fig. 5 for $n = 2, 3$. The results are compared to experimental data from the ALICE collaboration [68]. The presence of pre-equilibrium dynamics results in an increase of the integrated v_n coefficients. As a result, the free streaming and the EKT scenarios exhibit a better agreement to experimental data. This is unsurprising since the parameters were optimized for a system with prehydrodynamic evolution. It is nevertheless possible that equivalent agreement with experimental data could be achieved for the model without pre-equilibrium dynamics.

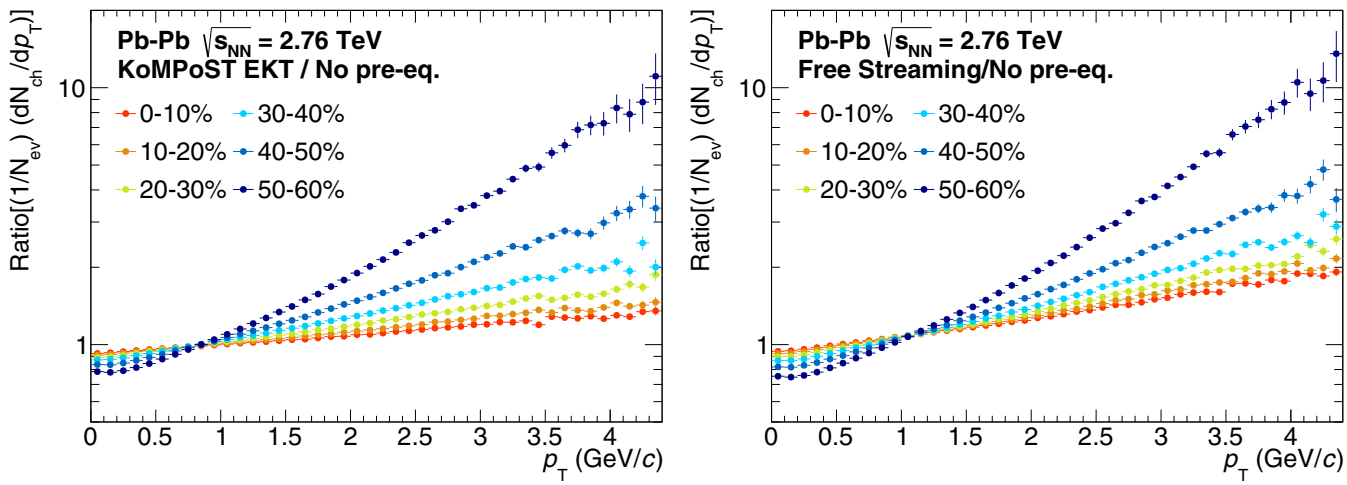

FIG. 3. Taking A defined above as the standard scenario, we plot the ratios of the momentum spectra from scenarios B (left) and C (right) with respect to scenario A as a function of the transverse momentum p_T.

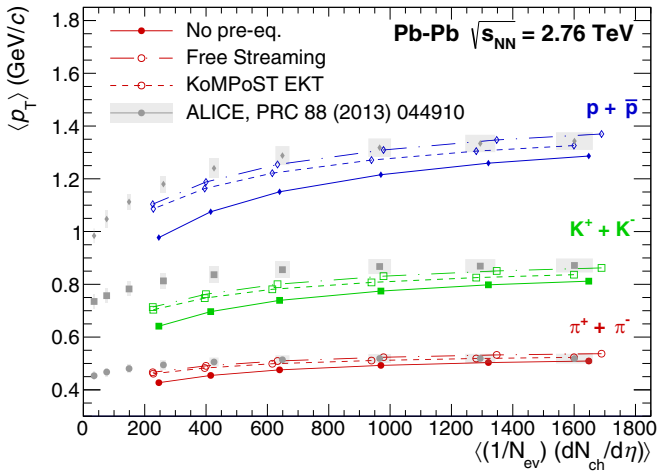

FIG. 4. Mean transverse momentum p_T for the three scenarios under investigation and for three sets of particle and antiparticle species: protons (blue), kaons (green), and pions (red), plotted as a function of the multiplicity of charged particles.

In principle, the origin of such increment in anisotropic flow could stem from a change in the transverse momentum dependence of these observables. To investigate this possibility and, more generally, to characterize flow fluctuations and momentum dependence of two-particle correlations, we have performed a principal component analysis (PCA) of the two-particle covariance matrix in transverse momentum $V_{n\Delta}$ [69–71].

This matrix can be written both in terms of its eigenvalues $\lambda_n^{(\alpha)}$ and normalized eigenvectors $\psi_n^{(\alpha)}(\mathbf{p})$, according to the spectral theorem, and in terms of its principal components $V_n^{(\alpha)}$,

$$\begin{aligned} V_{n\Delta}(\mathbf{p_1},\mathbf{p_2}) &\equiv \langle V_n^*(\mathbf{p_1}) V_n(\mathbf{p_2})\rangle \\ &= \sum_{\alpha=1}^{\infty} \lambda_n^{(\alpha)} \psi_n^{(\alpha)}(\mathbf{p}_a)\psi_n^{(\alpha)}(\mathbf{p}_b) \\ &= \sum_{\alpha=1}^{\infty} V_n^{(\alpha)}(\mathbf{p}_a) V_n^{(\alpha)}(\mathbf{p}_b). \end{aligned} \tag{9}$$

The principal components are then defined in terms of $\lambda_n^{(\alpha)}$ and $\psi_n^{(\alpha)}(\mathbf{p})$ as [69]

$$V_n^{(\alpha)} \equiv \sqrt{\lambda^{(\alpha)}}\psi_n^{(\alpha)}(\mathbf{p}). \tag{10}$$

While the leading principal component proxies the usual p_T-differential flow coefficient v_2, the subleading modes characterize flow correlations between two different transverse momenta [69].

In a recent work by the ExTrEme collaboration in Ref. [72], it was shown that the formalism proposed by Bhalerao *et al.* [69], in which the covariance matrix is written as

$$V_{n\Delta}^N(\mathbf{p}_a,\mathbf{p}_b) \equiv \frac{1}{(2\pi\,\Delta p_T\,\Delta y)^2}\left\langle \sum_{a\neq b} e^{-in(\phi_a-\phi_b)}\right\rangle, \tag{11}$$

suffers from contamination of the subleading principal components due to multiplicity fluctuations for $n > 0$. In the same work, an alternative prescription was proposed for performing the PCA analysis that removes such contaminations and makes it possible to isolate novel fluctuation sources, by diagonalizing, instead, the covariance matrix [72]

$$V_{n\Delta}^R(\mathbf{p}_a,\mathbf{p}_b) \equiv \frac{\left\langle \sum_{a\neq b} e^{-in(\phi_a-\phi_b)}\right\rangle}{\langle N_{\text{pairs}}(\mathbf{p}_a,\mathbf{p}_b)\rangle}. \tag{12}$$

We have performed such a PCA analysis for all the three scenarios simulated with our model for $n = 0$ following the proposal by Bhalerao *et al.* [69] and for $n = 2$ and $n = 3$ following the ExTrEme prescription (the $n = 0$ PCA analysis measures precisely multiplicity fluctuations, which are removed in the latter prescription). Results for selected centrality classes are presented in Figs. 6–8, and further results are presented in Figs. 13–15.[1]

It is clear from the plots that the measured PCA components are mostly insensitive to the type of pre-equilibrium dynamics utilized in the simulations. While this fact makes these observables particularly useful in isolating effects from the hydrodynamical evolution from effects of early stage dynamics, it also means that the source of the extra anisotropy in the integrated observables introduced by our models of pre-equilibrium dynamics does not stem from a possible change of the p_T dependence of the flow. The effect observed in integrated flow observables is indeed related to the changes in the transverse momentum spectra.

For flow, as in the case of the spectra, both the free streaming limit and the EKT scenario behave similarly. One may wonder whether there is a shared aspect to the free streaming and EKT scenarios that is responsible for this momentum increase. One such possibility is the fact that, like many models for the dynamics of the initial stages [27,28,60,74–77], both scenarios treat the evolution of massless particles. In fact, this system is conformally invariant and, thus, the trace of the energy-momentum tensor T^μ_μ necessarily vanishes everywhere, as already discussed. In terms of hydrodynamic variables, this means that the bulk pressure is zero and the total pressure in the kinetic approach is always given by $e/3$. In contrast, it is known that the QCD equation of state is not close to a conformal regime at the temperatures probed in fluid-dynamical simulations of heavy-ion collisions. If one assumes a continuous transition from a kinetic to a hydrodynamical regime, then this discontinuity in the thermodynamic pressure must be compensated by introducing an artificial discontinuity in the bulk pressure (which vanished exactly in KøMPøST). This means that the hydrodynamic evolution is always initialized with a positive bulk viscous pressure Π. That is, continuity of the energy-momentum tensor combined with a discontinuity of the thermodynamic equation of state demands a corresponding discontinuity in the bulk viscous

[1] A PCA analysis of the events generated with our model following the Bhalerao *et al.* prescription for $n = 2$ and $n = 3$ has been presented in a previous work [73].

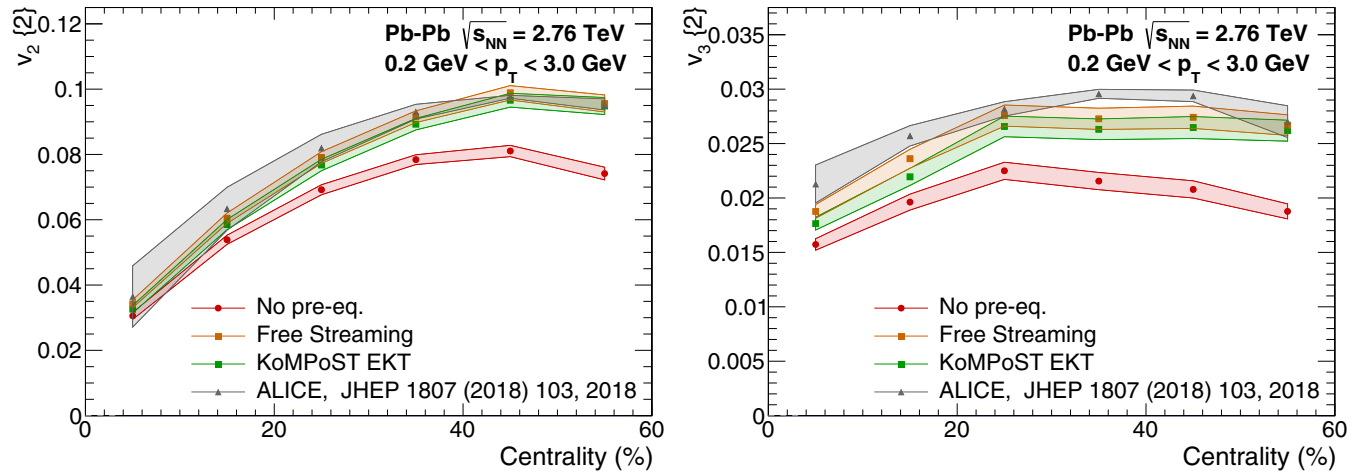

FIG. 5. Anisotropic flow coefficients from two particle correlations $v_2\{2\}$ (left) and $v_3\{2\}$ (right) for the three scenarios plotted as a function of event centrality.

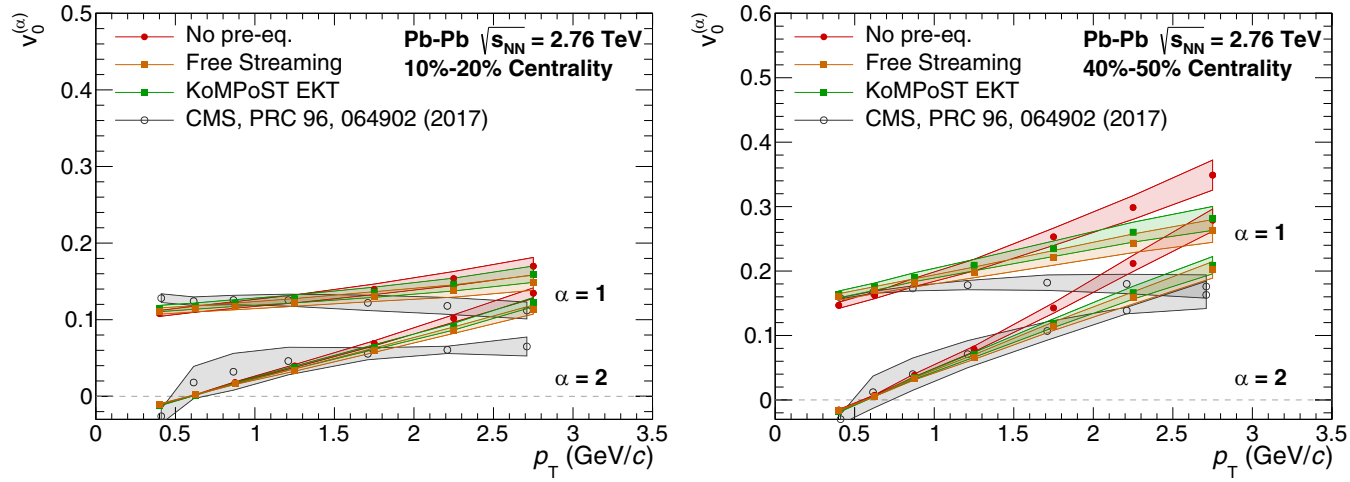

FIG. 6. First two principal components of the two-particle correlation matrix according to the prescription by Bhalerao *et al.* [69], for the harmonic $n = 0$ in the 10%–20% centrality class (left) and in the 40%–50% centrality classes (right) plotted as a function of the transverse momentum p_T.

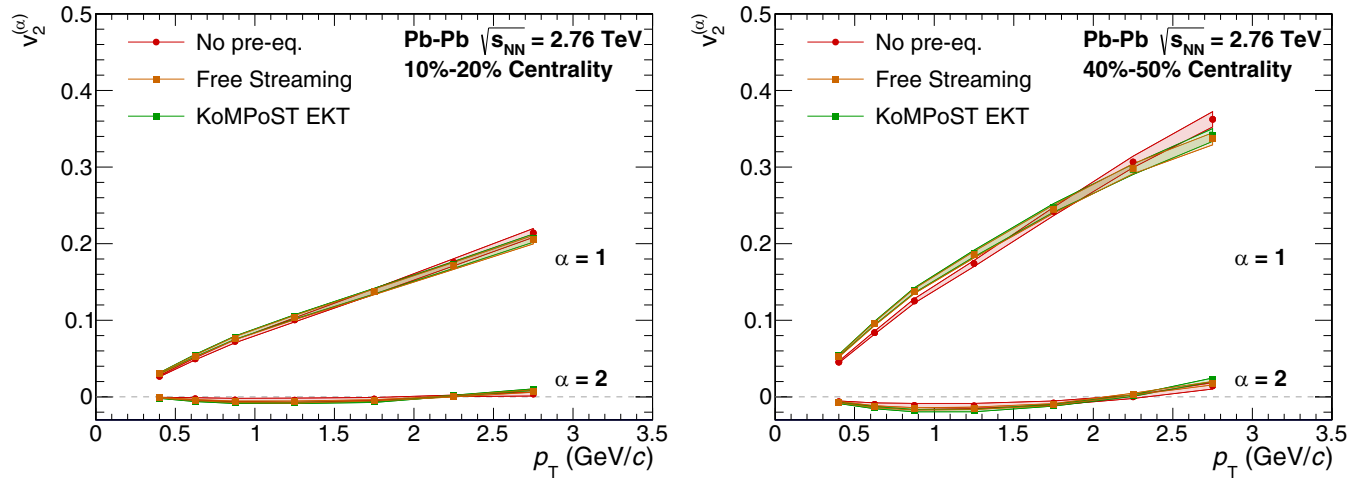

FIG. 7. First two principal components of the two-particle correlation matrix according to the ExTrEMe prescription [72], for the harmonic $n = 2$ in the 10%–20% centrality class (left) and in the 40%–50% centrality classes (right) plotted as a function of the transverse momentum p_T.

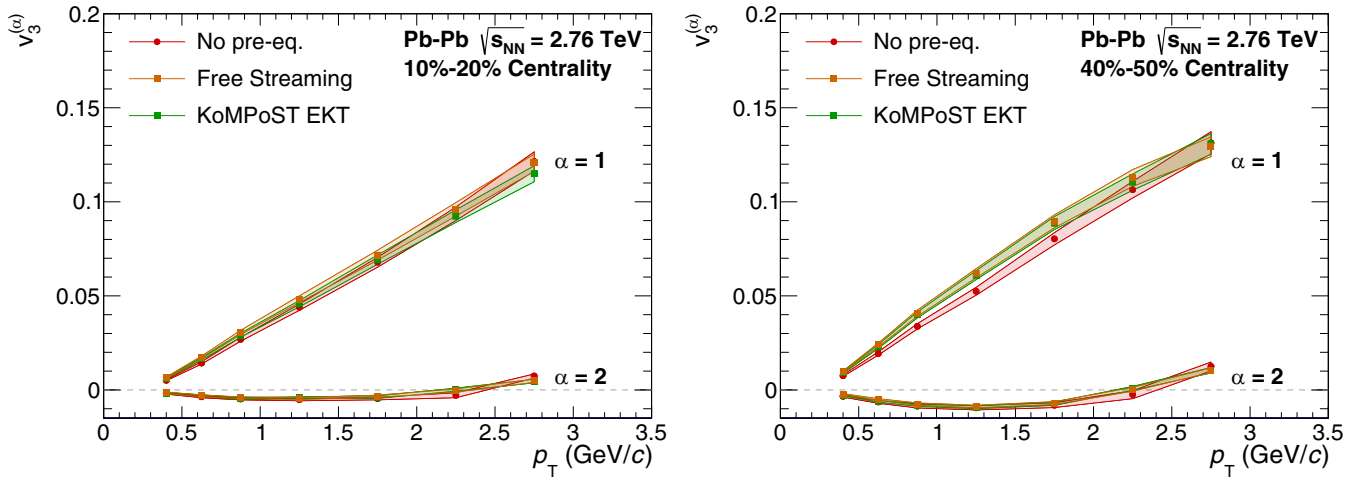

FIG. 8. First two principal components of the two-particle correlation matrix according to the ExTrEMe prescription [72], for the harmonic $n = 3$ in the 10%–20% centrality class (left) and in the 40%–50% centrality classes (right) plotted as a function of the transverse momentum p_T.

pressure. Specifically, this leads to the relation

$$\Pi + p(e) = \frac{e}{3}. \tag{13}$$

In Fig. 9 we show the ratio of bulk pressure to thermodynamic pressure $\Pi/p(e)$ as a function of energy density. Note that the conformal invariance of the prehydrodynamic model implies, via this matching, that the initial bulk pressure depends only the local energy density, and does not contain any information about the dynamics of the system. One can see that the bulk pressure can reach values larger than the QCD equilibrium pressure. We illustrate how this translates to our simulated events in Fig. 10, which shows that the bulk pressure at τ_{hydro} indeed reaches large positive values, especially near the edge of the system and in the majority of peripheral collision systems. This positive bulk pressure

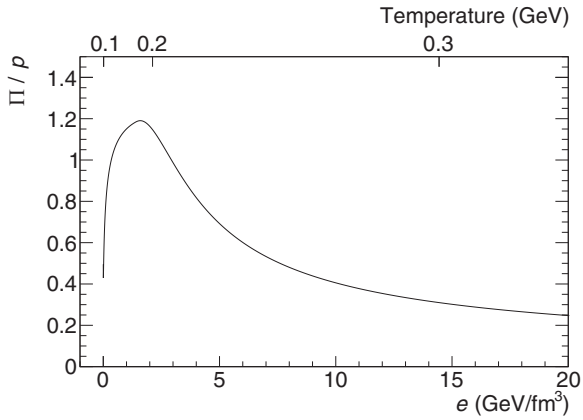

FIG. 9. Ratio between the bulk pressure Π and QCD thermodynamic pressure $p(e)$ implied by the equation of state s95o-v1.2 combined with the requirement that $T^{\mu}_{\mu} = 0$ at the hydrodynamization time, plotted as a function of the energy density e. The equivalent QCD temperature is also given for reference. See Eq. (13).

can indeed increase the radial expansion and, as a result, lead to larger mean transverse momentum. However, we note that this property is not realistic since conformal invariance is not a good approximation for QCD thermodynamics at these temperatures [64].

The question then arises how important is this unphysical aspect, and to what extent does it explain the observed change in p_T spectra? If it is responsible for a significant part of the observed increase in mean p_T, then this presents a significant problem, since the change in mean transverse momentum is the main notable effect of prehydrodynamic evolution. Further, this unrealistic feature is not exclusive to KøMPøST since it applies to all models that assume conformal invariance.[2]

To investigate this, we have performed new simulations, for a subset of 1000 of the original initial T$_{\text{R}}$ENTo profiles, for scenarios B and C (i.e., with KøMPøST in free streaming and EKT modes), but ignoring the bulk pressure at the hydrodynamization time (i.e., this quantity is set to zero at the beginning of hydrodynamical evolution). It should be noted that this procedure does not conserve energy and momentum, and we use it only as a rough estimate of the effect we want to study. We then compare final results for the mean transverse momentum with the results previously obtained by taking the ratios between both the EKT and free streaming scenarios to the baseline scenarios (without pre-equilibrium dynamics). The resulting average transverse momenta are presented in Fig. 11 and the ratios are shown in Fig. 12. Indeed, these results suggest that a significant fraction of the increase in $\langle p_T \rangle$ may come from the unphysically large bulk pressure at τ_{hydro}.

[2]As a matter of fact, KøMPøST represents an improvement over previous models, as it includes interactions among the quasiparticles.

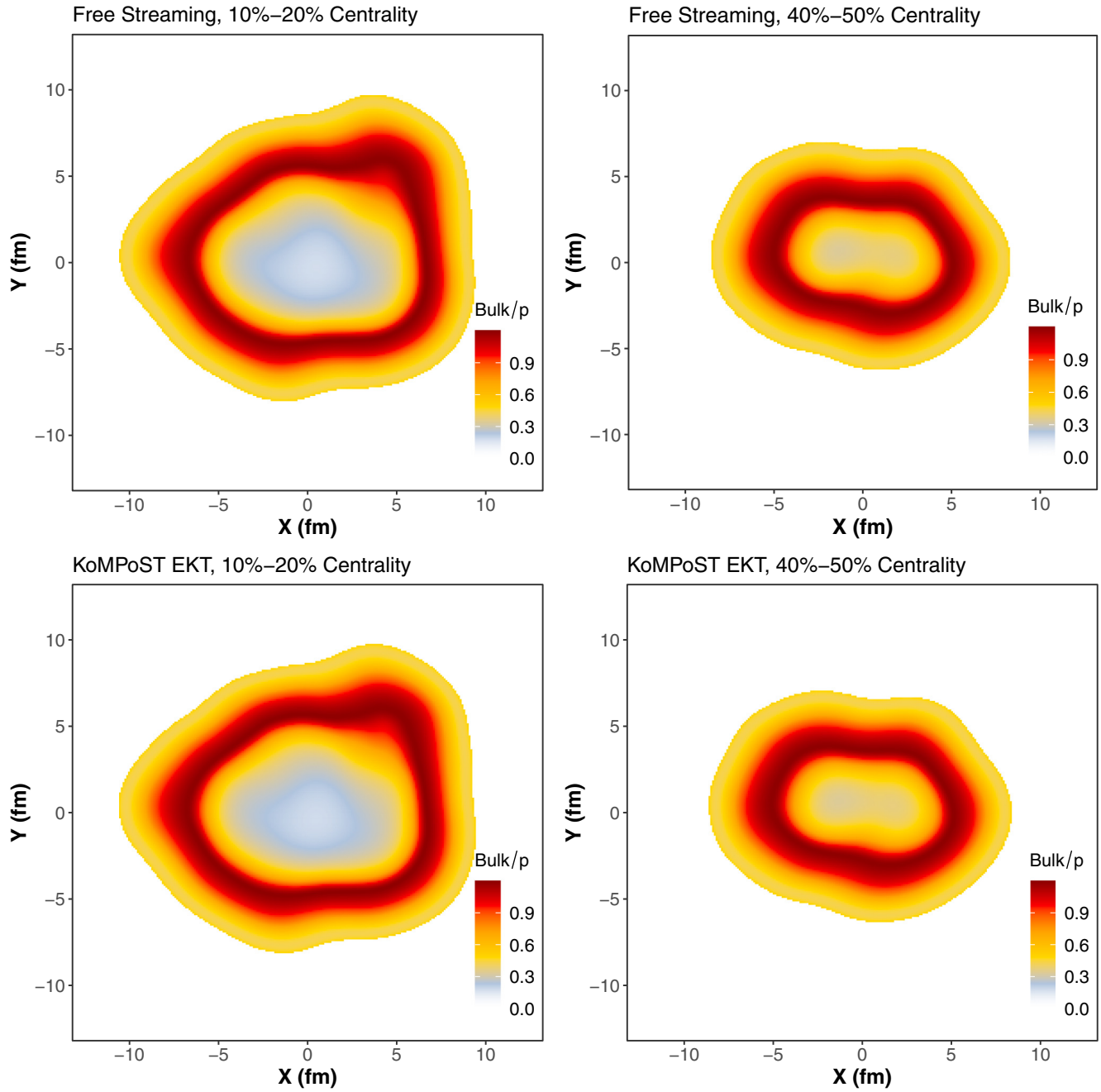

FIG. 10. Ratio Π/p extracted from sample events in different collision centralities classes and for both the free streaming (top) and EKT (bottom) scenarios at τ_{hydro}.

V. CONCLUSIONS AND OUTLOOK

In this work, we have studied how two different scenarios of pre-equilibrium dynamics, namely free streaming and effective kinetic theory implemented via KøMPøST, affect a collection of final-state observables in relativistic heavy-ion collisions employing a state-of-the-art model of heavy-ion collisions.

We found that the PCA observables, which were devised as a way to study flow fluctuations, are rather insensitive to the details of the pre-equilibrium dynamics and, moreover, to its inclusion in the hybrid model. This strengthens the use of PCA techniques of anisotropic flow as a powerful probe of the hydrodynamic evolution of the system. While the addition of a pre-equilibrium dynamic stage was in general found to be relevant for the calculation of some other observables, we have also found that a potentially large fraction of the observed effects may be an artifact of the underlying assumption of conformal invariance during pre-equilibrium evolution currently implemented in KøMPøST, which results in a large positive bulk pressure contribution to the pressure at the edges of the resulting initial condition of hydrodynamics at τ_{hydro}.

It will therefore be important in the future to relax the simplifying assumption of conformal invariance in models

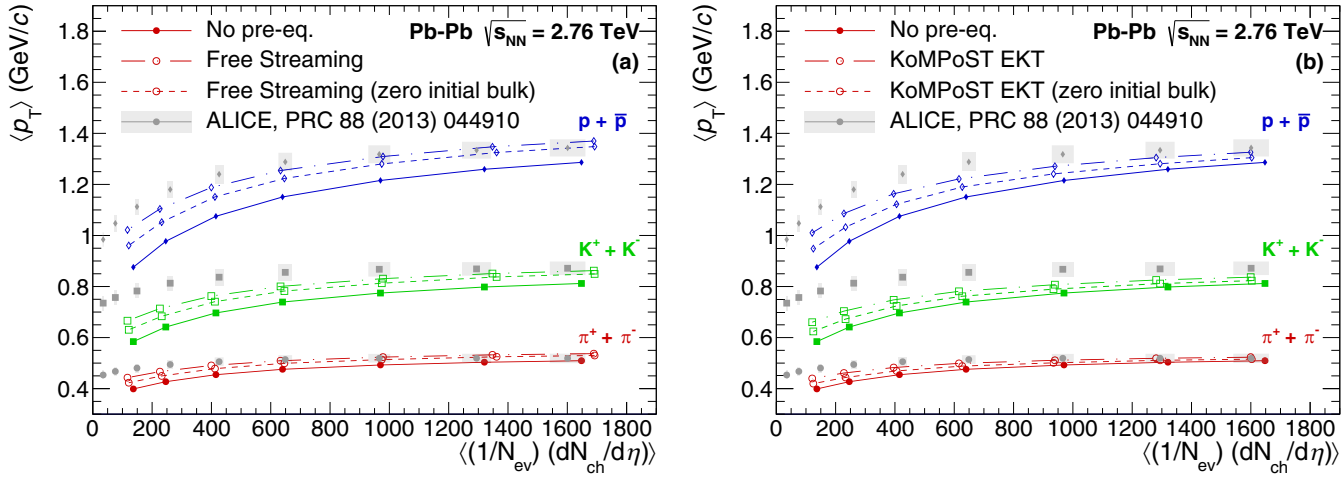

FIG. 11. Mean transverse momentum with full pre-equilibrium dynamics and with the bulk pressure set to zero at τ_{hydro}, plotted as a function of the charged particle multiplicity, for both free streaming (a) and EKT (b) scenarios. The scenario with no pre-equilibrium dynamics is also shown as a baseline case.

for the pre-equilibrium stage. We note that this is not a unique property of the KøMPøST model as it appears in any other model where simplifying approximations are made such that conformal invariance holds. In fact, a similar discussion is valid when using IP-Glasma generated initial conditions [27,28]. Also, this issue should affect the extraction of transport coefficients from analyses that employ a pre-equilibrium stage described by the evolution of massless partons, such as the Bayesian studies already cited in this work [60,74] and a recent study utilizing IP-Glasma initial conditions within a hybrid model [78]. While the size of the effect depends on the energy density (and, therefore, on τ_{hydro} where the description switches from conformal dynamics to nonconformal hydrodynamics), it is important to keep in mind that this unphysical effect exists when drawing conclusions from comparisons to experimental data using such models. In recent works [79,80] nonconformal effects were included in the prehydrodynamical phase by using a free streaming model with a variable velocity. The authors found that a breaking of conformal symmetry is preferred by a Bayesian analysis.

Nevertheless, it is important to remark that the general parts of the formalism developed in Refs. [33,34], which were based on causality and linear response, could in principle be implemented in other microscopic models that are not conformally invariant. In fact, a recent calculation of the Green's function which describes the evolution of energy and momentum perturbations for massless particles in the relaxation time approximation has yielded similar results to those obtained with KøMPøST [81]. Furthermore, in the context of kinetic models one may use a simple gas of particles with temperature dependent masses (in the relaxation time approximation) that can be engineered to describe basic QCD thermodynamic properties, see for instance [82]. Such a kinetic model would allow for a smooth transition to the hydrodynamic regime where T^{μ}_{μ} does not vanish at the beginning of the hydrodynamic evolution. However, in this approach one would most

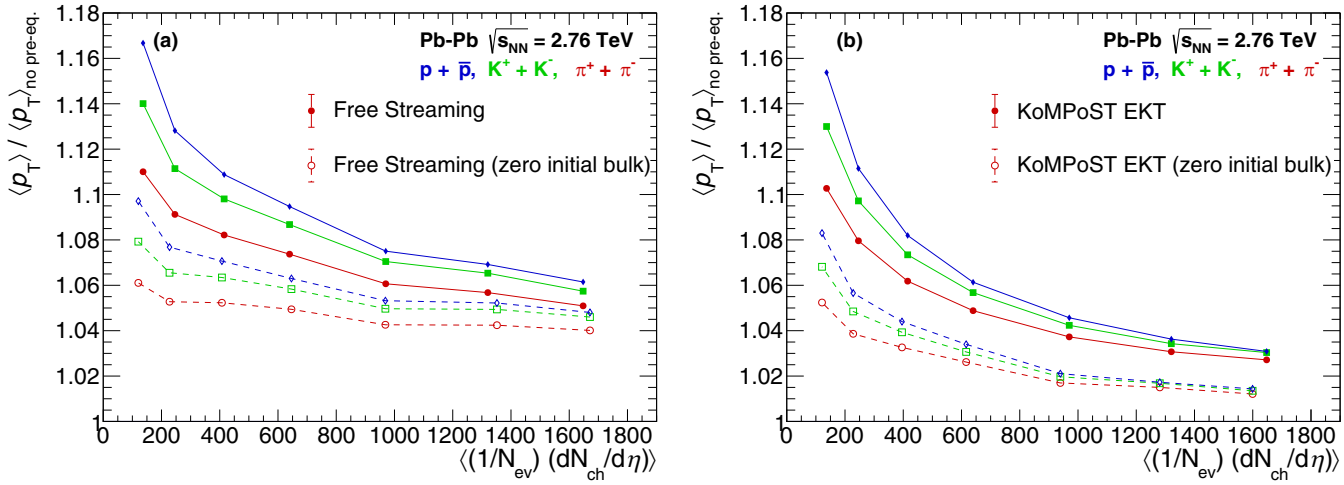

FIG. 12. Ratios of mean transverse momentum between scenarios with (painted symbols) and without (blank symbols) initial bulk pressure and the case without pre-equilibrium dynamics, plotted as a function of the charged particle multiplicity, for both Free Streaming (a) and EKT (b).

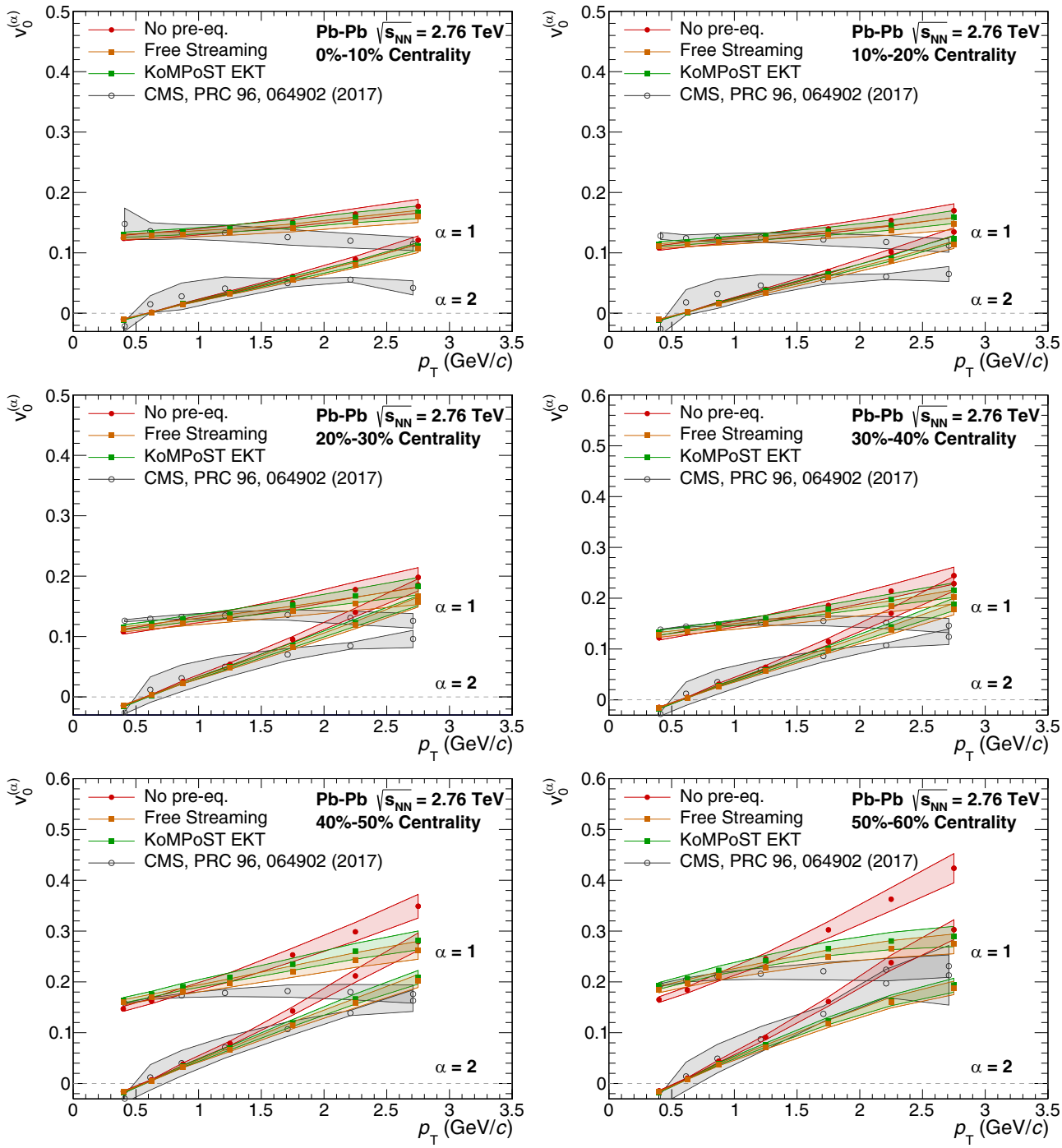

FIG. 13. First two principal components of the two-particle correlation matrix according to the prescription by Bhalerao *et al.* [69], plotted as a function of the transverse momentum p_T, for the harmonic $n = 0$ and several centrality classes.

certainly lose contact with QCD properties as such models can only be considered, at best, toy models for the nonconformal quark-gluon plasma formed in heavy-ion collisions. Another possibility could be to employ existing nonconformal transport approaches, such as PHSD [83,84], or BAMPS [85,86], to investigate the prehydrodynamical stage.

We note that in spite of our rescaling of the T$_R$ENTo profiles, as explained in Sec. III, an effect of the pre-equilibrium phase can still be seen as one moves to peripheral events in Fig. 1. This is most probably related to the evolution of the longitudinal pressure during this stage, as discussed in Ref. [87]. A detailed discussion of this effect, and its consequences to multiplicity fluctuations, will be deferred to future works. We further intend to explore different models of pre-equilibrium dynamics, aiming at resolving the issues related to the assumption of conformality, to provide a clearer picture of hydrodynamization in QCD matter. It is also interesting to explore in detail and quantify how different scenarios of

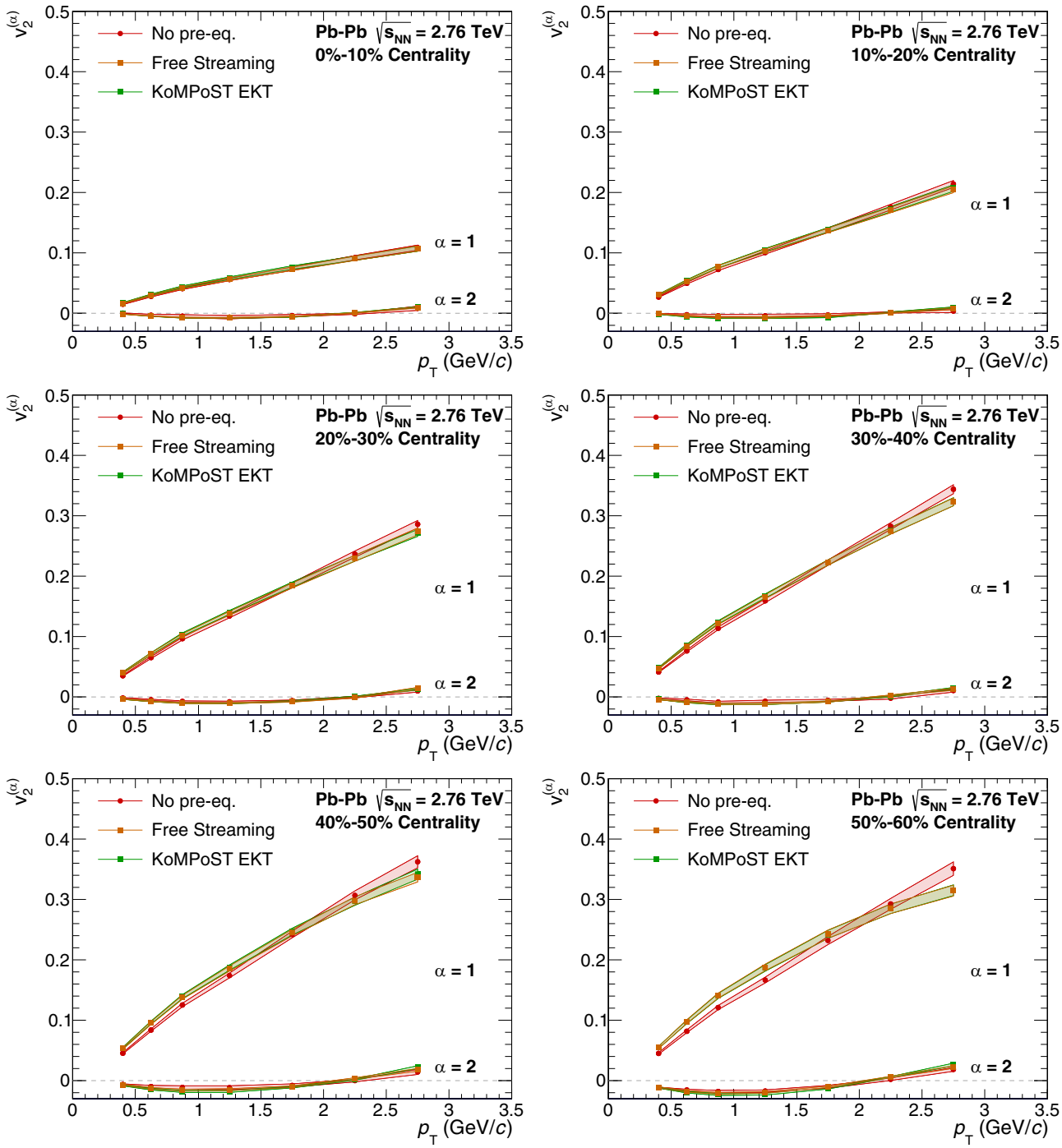

FIG. 14. First two principal components of the two-particle correlation matrix according to the ExTrEMe prescription [72], plotted as a function of the transverse momentum p_T, for the harmonic $n = 2$ and several centrality classes.

pre-equilibrium dynamics affect the extraction of transport coefficients, and to further confront these scenarios to experimental data.

ACKNOWLEDGMENTS

We thank J.-F. Paquet, A. Mazeliuaskas, and Soeren Schlichting for help with the technical numerical aspects within KøMPøST and for comments on a preliminary version of this manuscript. This research was funded by FAPESP Grants No. 2016/13803-2 (D.D.C.), No. 2016/24029-6, No. 2018/24720-6 (M.L.), No. 2017/05685-2 (all), No. 2018/01245-0 (T.N.dS.), and No. 2018/07833-1 (M.H.). D.D.C., M.L., G.S.D., and J.T. thank CNPq for financial support. G.S.D. acknowledges financial support from Fundação Carlos Chagas Filho de Amparo à

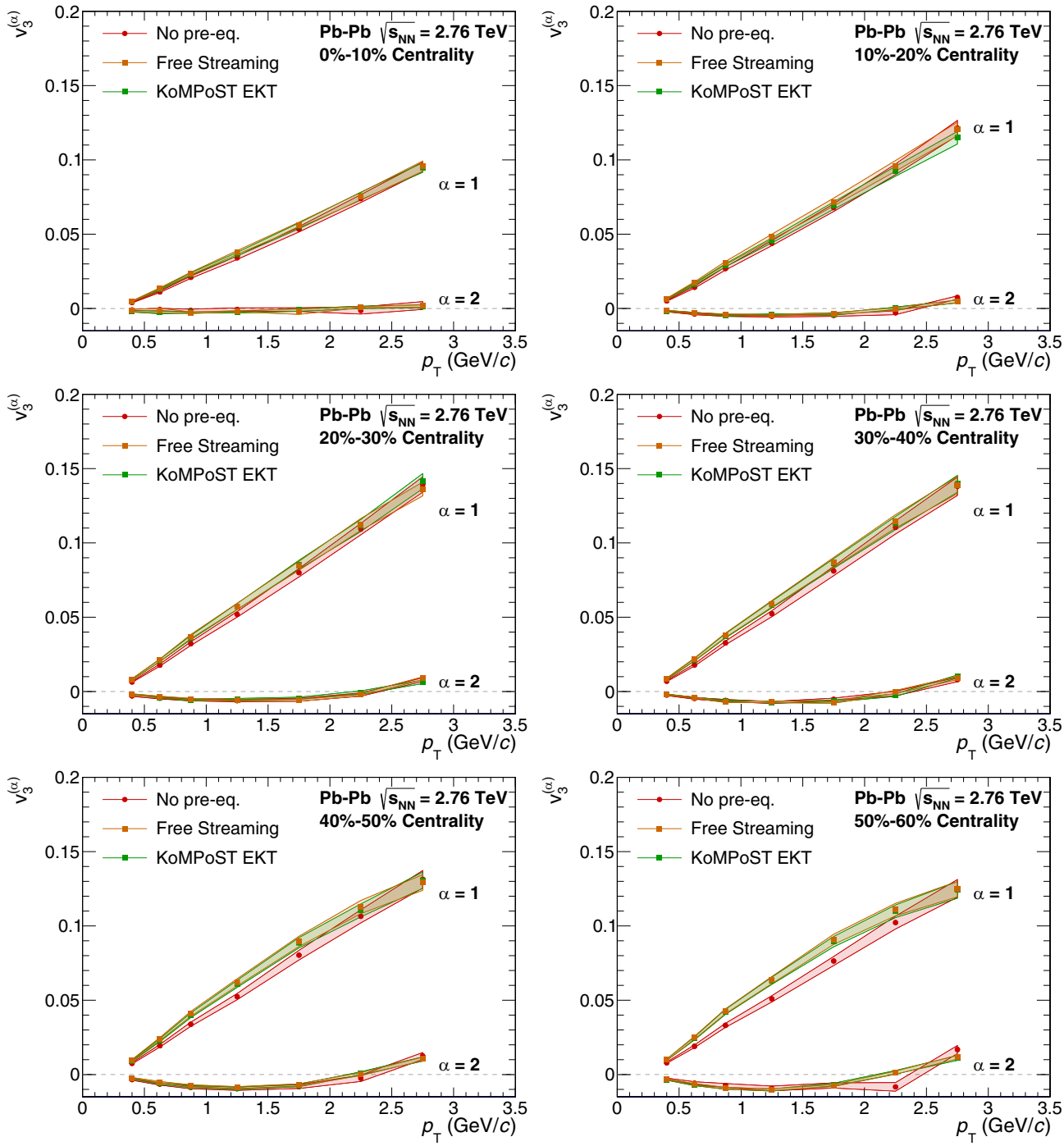

FIG. 15. First two principal components of the two-particle correlation matrix according to the ExTrEMe prescription [72], plotted as a function of the transverse momentum p_T, for the harmonic $n = 3$ and several centrality classes.

Pesquisa do Estado do Rio de Janeiro (FAPERJ), Grant No. E-26/202.747/2018. J.N. is partially supported by the US Department of Energy, Office of Science, Office for Nuclear Physics under Award No. DE-SC0021301. The authors also acknowledge computing time provided by the Research Computing Support Group at Rice University through agreement with the Universidade de São Paulo.

APPENDIX: CENTRALITY DEPENDENCE OF PCA RESULTS

For the sake of clarity, in this section we present the PCA results discussed in the main text for further centrality classes. These are presented in Figs. 13–15, for the $n = 0, 2, 3$ cases, for centrality classes going from 0–10% up to 50–60%.

[1] D. J. Gross and F. Wilczek, Phys. Rev. Lett. **30**, 1343 (1973).
[2] H. Politzer, Phys. Rev. Lett. **30**, 1346 (1973).
[3] E. V. Shuryak, Phys. Lett. B **78**, 150 (1978).
[4] J. C. Collins and M. Perry, Phys. Rev. Lett. **34**, 1353 (1975).
[5] E. Annala, T. Gorda, A. Kurkela, J. Nättilä, and A. Vuorinen, Nat. Phys. **16**, 907 (2020).
[6] I. Arsene *et al.* (BRAHMS Collaboration), Nucl. Phys. A **757**, 1 (2005).
[7] B. Back *et al.* (PHOBOS Collaboration), Nucl. Phys. A **757**, 28 (2005).
[8] K. Adcox *et al.* (PHENIX Collaboration), Nucl. Phys. A **757**, 184 (2005).
[9] J. Adams *et al.* (STAR Collaboration), Nucl. Phys. A **757**, 102 (2005).
[10] B. Muller, J. Schukraft, and B. Wyslouch, Annu. Rev. Nucl. Part. Sci. **62**, 361 (2012).
[11] P. Foka and M. A. Janik, Rev. Phys. **1**, 154 (2016).
[12] U. W. Heinz and M. Jacob, arXiv:nucl-th/0002042.
[13] U. Heinz and R. Snellings, Annu. Rev. Nucl. Part. Sci. **63**, 123 (2013).
[14] O. Philipsen, Prog. Part. Nucl. Phys. **70**, 55 (2013).
[15] R. Baier and P. Romatschke, Eur. Phys. J. C **51**, 677 (2007).
[16] H. Song and U. W. Heinz, Phys. Rev. C **77**, 064901 (2008).
[17] P. Romatschke and U. Romatschke, *Relativistic Fluid Dynamics In and Out of Equilibrium*, Cambridge Monographs on Mathematical Physics (Cambridge University Press, Cambridge, UK, 2019).
[18] H. Petersen, J. Steinheimer, G. Burau, M. Bleicher, and H. Stocker, Phys. Rev. C **78**, 044901 (2008).
[19] S. A. Bass and *et al.*, Prog. Part. Nucl. Phys. **41**, 255 (1998).
[20] M. Bleicher *et al.*, J. Phys. G **25**, 1859 (1999).
[21] M. L. Miller, K. Reygers, S. J. Sanders, and P. Steinberg, Annu. Rev. Nucl. Part. Sci. **57**, 205 (2007).
[22] C. Loizides, J. Nagle, and P. Steinberg, Software X **1-2**, 13 (2015).
[23] B. Zhang, C. M. Ko, B.-A. Li, and Z.-W. Lin, Phys. Rev. C **61**, 067901 (2000).
[24] Z.-W. Lin, C. M. Ko, B.-A. Li, B. Zhang, and S. Pal, Phys. Rev. C **72**, 064901 (2005).
[25] K. Werner, F.-M. Liu, and T. Pierog, Phys. Rev. C **74**, 044902 (2006).
[26] H. J. Drescher, F. M. Liu, S. Ostapchenko, T. Pierog, and K. Werner, Phys. Rev. C **65**, 054902 (2002).
[27] B. Schenke, P. Tribedy, and R. Venugopalan, Phys. Rev. Lett. **108**, 252301 (2012).
[28] B. Schenke, P. Tribedy, and R. Venugopalan, Phys. Rev. C **86**, 034908 (2012).
[29] J. S. Moreland, J. E. Bernhard, and S. A. Bass, Phys. Rev. C **92**, 011901(R) (2015).
[30] J. Weil *et al.*, Phys. Rev. C **94**, 054905 (2016).
[31] W. Broniowski, W. Florkowski, M. Chojnacki, and A. Kisiel, Phys. Rev. C **80**, 034902 (2009).
[32] J. Liu, C. Shen, and U. Heinz, Phys. Rev. C **91**, 064906 (2015); **92**, 049904(E) (2015).
[33] A. Kurkela, A. Mazeliauskas, J.-F. Paquet, S. Schlichting, and D. Teaney, Phys. Rev. C **99**, 034910 (2019).
[34] A. Kurkela, A. Mazeliauskas, J.-F. Paquet, S. Schlichting, and D. Teaney, Phys. Rev. Lett. **122**, 122302 (2019).
[35] J. Noronha-Hostler, G. S. Denicol, J. Noronha, R. P. G. Andrade, and F. Grassi, Phys. Rev. C **88**, 044916 (2013).
[36] J. Noronha-Hostler, J. Noronha, and F. Grassi, Phys. Rev. C **90**, 034907 (2014).
[37] C. Shen, Z. Qiu, H. Song, J. Bernhard, S. Bass, and U. Heinz, Comput. Phys. Commun. **199**, 61 (2016).
[38] B. Schenke, S. Jeon, and C. Gale, Phys. Rev. C **82**, 014903 (2010).
[39] B. Schenke, S. Jeon, and C. Gale, Phys. Rev. C **85**, 024901 (2012).
[40] J.-F. Paquet, C. Shen, G. S. Denicol, M. Luzum, B. Schenke, S. Jeon, and C. Gale, Phys. Rev. C **93**, 044906 (2016).
[41] F. Cooper and G. Frye, Phys. Rev. D **10**, 186 (1974).
[42] S. Pratt and G. Torrieri, Phys. Rev. C **82**, 044901 (2010).
[43] P. Huovinen and H. Petersen, Eur. Phys. J. A **48**, 171 (2012).
[44] S. Pratt, Phys. Rev. C **89**, 024910 (2014).
[45] M. Chojnacki, A. Kisiel, W. Florkowski, and W. Broniowski, Comput. Phys. Commun. **183**, 746 (2012).
[46] H. Petersen, D. Oliinychenko, M. Mayer, J. Staudenmaier, and S. Ryu, Nucl. Phys. A **982**, 399 (2019).
[47] A. Mazeliauskas, S. Floerchinger, E. Grossi, and D. Teaney, Eur. Phys. J. C **79**, 284 (2019).
[48] W. Florkowski, M. P. Heller, and M. Spalinski, Rep. Prog. Phys. **81**, 046001 (2018).
[49] J. Berges, M. P. Heller, A. Mazeliauskas, and R. Venugopalan, arXiv:2005.12299.
[50] V. Khachatryan *et al.* (CMS Collaboration), J. High Energy Phys. 09 (2010) 091.
[51] B. Abelev *et al.* (ALICE Collaboration), Phys. Lett. B **719**, 29 (2013).
[52] L. D. McLerran and R. Venugopalan, Phys. Rev. D **49**, 2233 (1994).
[53] J. D. Bjorken, Phys. Rev. D **27**, 140 (1983).
[54] P. B. Arnold, G. D. Moore, and L. G. Yaffe, J. High Energy Phys. 01 (2003) 030.
[55] L. D. Landau and E. M. Lifshitz, in *Fluid Mechanics—Volume 6 (Course of Theoretical Physics)*, 2nd ed. (Butterworth-Heinemann, Oxford, UK, 1987), p. 552.
[56] W. Israel, Ann. Phys. **100**, 310 (1976).
[57] W. Israel and J. Stewart, Ann. Phys. **118**, 341 (1979).
[58] S. Ryu, J. F. Paquet, C. Shen, G. S. Denicol, B. Schenke, S. Jeon, and C. Gale, Phys. Rev. Lett. **115**, 132301 (2015).
[59] J. E. Bernhard, J. S. Moreland, S. A. Bass, J. Liu, and U. Heinz, Phys. Rev. C **94**, 024907 (2016).
[60] J. E. Bernhard, Ph.D. thesis, Duke University (2018).
[61] K. Aamodt *et al.* (ALICE Collaboration), Phys. Rev. Lett. **106**, 032301 (2011).
[62] P. Huovinen and P. Petreczky, Nucl. Phys. A **837**, 26 (2010).
[63] A. Bazavov *et al.*, Phys. Rev. D **80**, 014504 (2009).
[64] P. Alba, V. Mantovani Sarti, J. Noronha, J. Noronha-Hostler, P. Parotto, I. Portillo Vazquez, and C. Ratti, Phys. Rev. C **98**, 034909 (2018).
[65] P. Alba *et al.*, Phys. Rev. D **96**, 034517 (2017).
[66] N. Borghini, P. M. Dinh, and J.-Y. Ollitrault, Phys. Rev. C **64**, 054901 (2001).
[67] A. Bilandzic, R. Snellings, and S. Voloshin, Phys. Rev. C **83**, 044913 (2011).
[68] S. Acharya *et al.* (ALICE Collaboration), J. High Energy Phys. 07 (2018) 103.
[69] R. S. Bhalerao, J. Y. Ollitrault, S. Pal, and D. Teaney, Phys. Rev. Lett. **114**, 152301 (2015).

[70] A. Mazeliauskas and D. Teaney, Phys. Rev. C **93**, 024913 (2016).
[71] A. Mazeliauskas and D. Teaney, Phys. Rev. C **91**, 044902 (2015).
[72] M. Hippert, D. Dobrigkeit Chinellato, M. Luzum, J. Noronha, T. Nunes da Silva, and J. Takahashi, Phys. Rev. C **101**, 034903 (2020).
[73] T. N. da Silva, D. D. Chinellato, R. D. de Souza, M. Hippert, M. Luzum, J. Noronha, and J. Takahashi, Proceedings **10**, 5 (2019).
[74] J. E. Bernhard, J. S. Moreland, and S. A. Bass, Nat. Phys. **15**, 1113 (2019).
[75] P. Romatschke, Eur. Phys. J. C **75**, 305 (2015).
[76] R. D. Weller and P. Romatschke, Phys. Lett. B **774**, 351 (2017).
[77] D. Everett *et al.* (JETSCAPE Collaboration), arXiv:2011.01430.
[78] C. Gale, J.-F. Paquet, B. Schenke, and C. Shen, Nucl. Phys. A **1005**, 121863 (2021).
[79] G. Nijs, W. van der Schee, U. Gürsoy, and R. Snellings, arXiv:2010.15130.
[80] G. Nijs, W. Van Der Schee, U. Gürsoy, and R. Snellings, arXiv:2010.15134.
[81] S. Kamata, M. Martinez, P. Plaschke, S. Ochsenfeld, and S. Schlichting, Phys. Rev. D. **102**, 056003 (2020).
[82] M. Alqahtani, M. Nopoush, and M. Strickland, Phys. Rev. C **92**, 054910 (2015).
[83] W. Cassing and E. L. Bratkovskaya, Phys. Rev. C **78**, 034919 (2008).
[84] W. Cassing and E. L. Bratkovskaya, Nucl. Phys. A **831**, 215 (2009).
[85] Z. Xu and C. Greiner, Phys. Rev. C **71**, 064901 (2005).
[86] Z. Xu and C. Greiner, Phys. Rev. C **76**, 024911 (2007).
[87] G. Giacalone, A. Mazeliauskas, and S. Schlichting, Phys. Rev. Lett. **123**, 262301 (2019).